15th Triennial World Congress, Barcelona, Spain

KINETIC MODELLING OF NICOTINIC ACETYLCHOLINE RECEPTORS WITH 5-[^{123}I]IODO-A-85380 AND DYNAMIC SINGLE-PHOTON EMISSION COMPUTED TOMOGRAPHY [1]

Koon-Pong Wong [*,**] **Stefan Eberl** [*] **David D. Feng** [**,***]
Michael Kassiou [*,****] **Michael J. Fulham** [*,†]

[*] *Department of PET and Nuclear Medicine*
Royal Prince Alfred Hospital, NSW 2050, Sydney, Australia
[**] *School of Information Technologies*
The University of Sydney, NSW 2006, Sydney, Australia
[***] *Department of Electronic and Information Engineering*
The Hong Kong Polytechnic University, Hong Kong
[****] *Department of Pharmacology*
The University of Sydney, NSW 2006, Sydney, Australia
[†] *Faculty of Medicine*
The University of Sydney, NSW 2006, Sydney, Australia

Abstract: 5-iodo-3-(2(S)-azetidinylmethoxy)pyridine (5-[^{123}I]iodo-A-85380) is a novel radioligand for brain nicotinic acetylcholine receptors (nAChRs), having demonstrated high specific binding to nAChRs and favourable properties for *in vivo* imaging. The purpose of this study was to evaluate different tracer kinetic modelling strategies for the quantification of regional nAChR binding in baboon brain using dynamic single-photon emission computed tomography (SPECT). Imaging studies were performed on two anaesthetised baboons. The radioligand (397±43 MBq) was infused into the animals over 2 min and dynamic SPECT images were acquired for 3 hr. The plasma input function was determined from arterial blood samples with metabolite correction. The data were analysed using 2- and 3-compartment models. Reliable fits could be obtained with a 3-compartment model which provided significantly improved fitting as compared to the 2-compartment model, despite poor identifiability in some parameters. The 2-compartment model failed to fit the data adequately even though the identifiability of parameters was high. The 3-compartment model described the data well, and with the strategies used to obtain reliable fits, is the model of choice for analysis of 5-[^{123}I]iodo-A-85380 kinetics. *Copyright © 2002 IFAC*

Keywords: Binding, biomedical systems, modelling, parameter estimation.

1. INTRODUCTION

Neuronal nicotinic acetylcholine receptors (nAChRs) are thought to play an important role in tabacoo dependence (Corrigall *et al.*, 1992) and are affected in various neurodegenerative conditions such as Alzheimer's and Parkinson's diseases (Perry *et al.*, 1995). These receptors are also involved in different CNS functions, for instance, learning and memory (Levin and Rose, 1995). *In vivo* studies of nAChRs, however, have been limited by the lack of suitable radiotracers for imaging. Initial attempt to study nAChRs in the living brain with positron emission tomography (PET) was made possible by using [^{11}C]-nicotine but rapid washout of the tracer from the brain and high degree of nonspecific binding impede its applications

[1] This work was supported by the National Health and Medical Research Council of Australia under Grant 980042; by the Australian Research Council under Grant A10009011; and by the University Grant Council of Hong Kong.

for quantitative *in vivo* studies (Nybäck *et al.*, 1994). Current research efforts have focused on development of new, highly specific and selective nAChR radioligands that are capable of localising nAChRs *in vivo* with high affinity. The discovery of epibatidine, a potent nAChR agonist, has stimulated development of nAChR radioligands with favourable properties for imaging with PET and single-photon emission computed tomography (SPECT). However, the high toxicity of epibatidine-related compounds may preclude their use in human studies (Molina *et al.*, 1997).

A series of 3-pyridyl ether compounds possessing subnanomolar affinity for nAChRs with reduced toxicity profile has been reported recently. One of these compounds, 3-(2(S)-azetidinylmethoxy)pyridine (A-85380) possesses high affinity for $\alpha 4\beta 2$ nAChRs in human. It has been labelled with iodine-123 (5-[^{123}I]iodo-A-85380) and demonstrated high specificity and selectivity for nAChRs in mouse brain *in vivo*, with low acute toxicity (Musachio *et al.*, 1998). 5-[^{123}I]iodo-A-85380 has also been used in SPECT imaging of nAChRs in Rhesus monkey and Papio anubis baboon (Chefer *et al.*, 1998; Musachio *et al.*, 1999). We have recently described our methodology for imaging nAChR binding using 5-[^{123}I]iodo-A-85380 and SPECT and reported the first *in vivo* imaging of nAChR upregulation in response to chronic (-)-nicotine treatment in baboon (Kassiou *et al.*, 2001). The aim of this study was to investigate different tracer kinetic modelling strategies for the quantification of 5-[^{123}I]iodo-A-85380 in baboon brain using SPECT.

2. METHODS

2.1 *Radioligand synthesis*

Full details of 5-[^{123}I]iodo-A-85380 synthesis have been described previously (Kassiou *et al.*, 2001).

2.2 *Animal Preparation*

The study procedures were approved by the Central Sydney Area Health Service Animal Welfare Committee. Two adult male *Papio hamadryas* baboons were studied pre- and post-chronic treatment with saline or (-)-nicotine. The (-)-nicotine treated baboon (Evan) weighed 23.6 kg and the weight of the saline control baboon (Max) was 21.3 kg. After the baseline imaging study for the baboons, subcutaneously implanted osmotic pumps (Alzet 2ML2, Alza Corporation, Palo Alto, CA, USA) were used to infuse a saline solution of (-)-nicotine tartrate (2 mg/kg/24hr) for Evan and saline for Max, continuously during a 14 day period. Prior to pump implantation, animals were anaesthetised with ketamine (5–8 mg, intramuscular injection). Venous blood samples were taken from both animals at baseline, 2 days, and 15 days after pump implantation, and 7 days after the pump had been removed for Evan. Plasma samples were then analysed to determine the levels of (-)-nicotine and cotinine in plasma.

2.3 *Data Acquisition*

The experimental conditions and injected dose are summarised in Table 1. Animals were anaesthetised with ketamine (5–8 mg, intramuscularly), and anaesthesia was maintained throughout the study by infusion of ketamine (13 mg/kg/hr). Baboons were placed in a Trinoix Triad XLT triple head gamma camera (Trionix Research Laboratory, Twinsburg, OH) and the head was immobilised in the head holder using a thermoplastic mask. A 15-min transmission scan with a line source filled with ^{99m}Tc at the focus of a long focal length (1140 mm) fan beam collimator was performed prior to tracer administration and was used for photon attenuation correction. Dynamic emission SPECT imaging was performed with ultra high resolution, low energy (UHR-LE) short focal length (480 mm) fan beam collimators fitted to all three detectors.

Dynamic emission data acquisition and arterial blood sampling were commenced simultaneously with the start of a 2 min infusion of the ligand using a syringe pump. Data were sampled every 30 s at the beginning and were gradually extended to every 5 and 10 min for a total data acquisition time of 3 hrs. Data were collected into 128×64 projection images (pixel size = 3.6 mm $\times$ 3.6 mm) with continuous rotation and binning into 60 projections for a complete rotation. The 30 s frames were integrated into 1 min frames for further processing. Fan beam data were rebinned to parallel beam data with a zoom of 1.6, resulting in a final isotropic reconstructed voxel size of 2.2 mm $\times$ 2.2 mm $\times$ 2.2 mm.

2.4 *Plasma Metabolite Analysis and Input Function*

Arterial blood samples were taken throughout the study. The samples were centrifuged for 5 min at 5000 rpm to separate plasma for counting in an automated NaI well counter which was cross calibrated with the SPECT system by counting aliquots of a phantom filled with a ^{123}I solution of known activity and by acquiring and processing SPECT studies of the phantom on the gamma camera similar to the baboon studies. Aliquots of plasma samples taken at 2, 5, 10, 15, 30 and 180 min were used to determine the metabolite fraction in plasma by acetonitrile denaturation followed by TLC. The measured unmetabolised fractions were fitted with a dual exponential function and all plasma sample counts were corrected for metabolites using the fitted curve. The metabolite corrected data were decay corrected and cross calibrated to produce the input function for kinetic modelling.

2.5 *Image Analysis*

Emission data were corrected for scatter using transmission dependent scatter correction (Narita *et al.*, 1997) and reconstructed using the ordered-subset expectation-maximisation (OSEM) iterative (2 iterations, 20 subsets) reconstruction algorithm (Hudson

Table 1. Experimental conditions and injected dose for the treated baboon (Evan) and the control baboon (Max).

Study	Experimental condition	Dose injected
$Evan_{baseline}$	Baseline, prior to any treatment	400 MBq
$Evan_{nicotine}$	End of chronic (-)-nicotine treatment, pump removed at end of scan	447 MBq
$Evan_{post1}$	Day 7 post (-)-nicotine treatment and pump removal	392 MBq
$Evan_{post2}$	Week 5 post (-)-nicotine treatment and pump removal	390 MBq
$Max_{baseline}$	Baseline, prior to any treatment	434 MBq
Max_{saline}	Day 15 of saline treatment, pump removed at end of scan	324 MBq
Max_{post1}	Week 4 post saline treatment and pump removal	197 MBq

and Larkin, 1994). Attenuation was corrected with attenuation maps derived from the transmission scan. The reconstructed images were then convolved with a three-dimensional Gaussian kernel with a full-width at half-maximum of 3.7 mm. The resultant SPECT images were cross calibrated with the NaI well counter. One of the baseline studies was selected as a reference study for each baboon and was resliced along planes parallel to the orbito-meatal line. The other studies were coregistered to the resliced reference study using an automated image registration algorithm (Eberl *et al.*, 1996). Volumes of interest (VOIs) were placed manually on the frontal cortex and cerebellum in the summation of the first 40 min of the reference study images and were applied to all coregistered studies. The thalamus VOIs were automatically defined by taking the highest 300 connected voxels in the summation of the images acquired from 150 to 180 min post radioligand infusion. Automated VOI delineation failed in the nicotinic treatment study, where thalamus uptake was not prominent. The thalamus VOI in the reference study was applied instead.

2.6 *Compartmental Model Fitting*

Tissue time-activity curves (TACs) generated for each VOI were investigated with both 2-compartment and 3-compartment models using nonlinear least squares fitting and the metabolite corrected input function, under the assumptions that labelled metabolites in the plasma do not cross the blood-brain barrier and that there are either low amount of metabolites produced in the brain and/or they egress rapidly from the brain, similar to the non-specific uptake. Therefore the labelled metabolite in tissue is negligible. Figure 1 shows the structures of the 3-compartment and 2-compartment models. Rate constants (K_1, k_2, k_2', k_3, and k_4) were estimated by model fitting and cerebral blood volume was assumed to be 5% in all regions. The volume of distribution (V_d), the binding potentials, BP_1 (Mintun *et al.*, 1984), and BP_2 (Laruelle *et al.*, 1994) for the 3-compartment model were calculated according to the following equations:

$$V_d = \frac{K_1}{k_2}\left(1 + \frac{k_3}{k_4}\right) \tag{1}$$

$$BP_1 = \frac{k_3}{k_4} \tag{2}$$

$$BP_2 = \frac{K_1 k_3}{k_2 k_4} \tag{3}$$

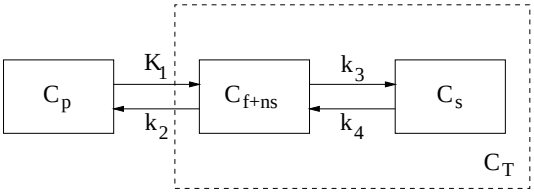

(a) 3-compartment model

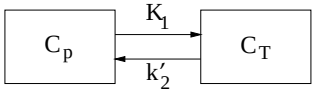

(b) 2-compartment model

Fig. 1. Kinetic models used in compartmental model fitting. C_p, arterial plasma concentration; C_{f+ns}, concentration of free and non-specifically bound ligand in tissue; C_s, concentration of specifically bound ligand in tissue; C_T, total activity concentration in tissue.

BP_1 is claimed to represent the ratio of the two tissue compartment volumes. BP_2 has been shown to represent the volume of the specific binding compartment (Laruelle *et al.*, 1994). However, it explicitly contains the tracer delivery and influx rate constant (K_1) which may confound the results, particularly when K_1 is affected by the treatment. The following equation was used to calculate the volume of distribution (V_d') for the 2-compartment model:

$$V_d' = \frac{K_1}{k_2'} \tag{4}$$

but the binding potential could not be determined for this model.

As highlighted by Fujita *et al.* (2000), reliability of fitting the 3-compartment model can be problematic. The following strategies were thus employed to constrain the 3-compartment model fit: (1) The 2-compartment model was always fitted first and the initial values for the 3-compartment model were derived from the parameters obtained from the 2-compartment model fit. (2) The residual sum of square (RSSQ) from the 3-compartment model fit had to be less than 1.1×RSSQ of the 2-compartment model fit. (3) V_d for 3-compartment model fit was constraint to be less than two times the V_d estimated by the 2-compartment model fit. (4) The mean parameter values of the 100 bootstrap Monte Carlo realisations provided improved

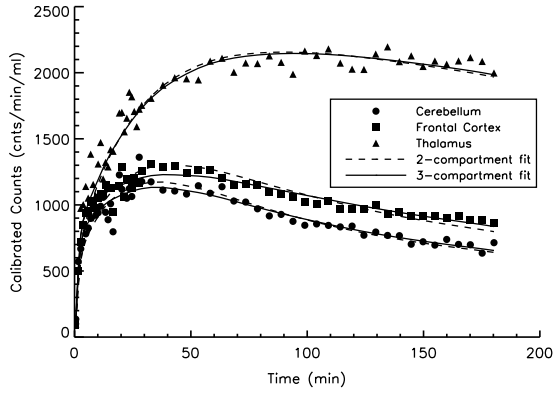

Fig. 2. Plots of tissue TACs for the cerebellum, frontal cortex, and thalamus in $\text{Evan}_{\text{baseline}}$, and their corresponding 2- and 3-compartment model fits.

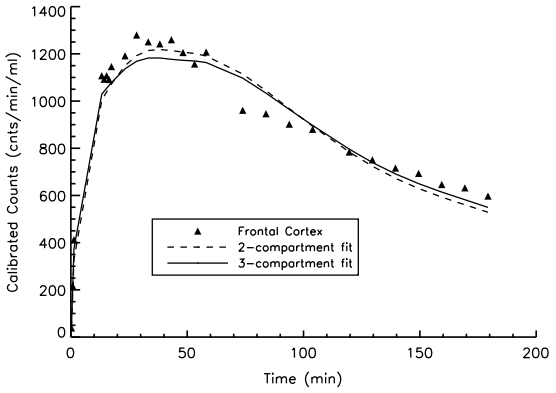

Fig. 3. Plot of tissue TACs for the frontal cortex in Max at baseline level ($\text{Max}_{\text{baseline}}$). Corresponding 2- and 3-compartment model fits are also shown.

estimate of parameters. Given a curve of n data points, for each of bootstrap Monte Carlo iteration, n points are randomly selected from the curve and the model is fitted to the n randomly selected points. As the n points are randomly selected, some of the points from the original data set will be duplicated while others will not be selected. The points which are duplicated and not selected will vary randomly for each iteration (Press *et al.*, 1992).

2.7 *Statistical Analysis*

The standard deviations (SD) of the rate constants and macroparameters (V_d', V_d, BP_1 and BP_2) were derived from the bootstrap Monte Carlo technique with 100 iterations. The identifiability of the parameter is defined by the coefficient of variation (CV), which is defined as the ratio of SD to the value of the parameter estimate. To statistically compare the adequacy of the model fits, the F-statistic (Landaw and DiStefano, 1984), the Akaike Information Criterion (Akaike, 1974) and the Schwarz Criterion (Schwarz, 1978) were computed for each model configuration. For the F-statistic, the null hypothesis that the lower-order model (2-compartment model in this study) fits the data better is rejected if the probability is less than an acceptable level ($P < 0.05$ was chosen). As for the Akaike Information Criterion (AIC) and the Schwarz Criterion (SC), the model configuration with the lowest score is preferred. Nonparametric run test was also used to test whether the residuals between the measurements and the fitted data points were randomly distributed above zero. Differences with $P < 0.05$ were considered statistically significant.

3. RESULTS AND DISCUSSION

Figure 2 shows the tissue TACs of the cerebellum, frontal cortex and thalamus for one of the baseline studies ($\text{Evan}_{\text{baseline}}$). The corresponding 2- and 3-compartment model fits are also shown. The increased uptake and retention of 5-[^{123}I]iodo-A-85380 in the thalamus as compared to the other regions are clearly evident. The regional distribution of the radioligand was also consistent with the known densities of nAChRs in baboon brain (thalamus > frontal cortex > cerebellum). It was apparent that 2-compartment model failed to fit the data adequately, as shown in this figure.

Tables 2 and 3 summarise the compartmental model fitting results for both 2- and 3-compartment models. The CV of the parameters estimated with the 2-compartment model in all cases was <10% except the thalamus curve of $\text{Max}_{\text{baseline}}$ where the CV of k_2' was 13%. The reliability in estimating K_1 using the 3-compartment model was reasonable, with CV <10% for all fits. The CV of the rate constant parameters estimated with the 3-compartment model, was generally higher (i.e. lower reliability) as compared to the corresponding 2-compartment model fitting. Some high correlations ($r \approx 0.95$) between parameters were observed with the 3-compartment model fits but $r > 0.9$ was also seen between parameters in 2-compartment model fits. The high correlations between and low reliability of the rate constant parameters suggested that more than 3 compartments would not be able to fit the data. This is in agreement with the recent findings of Fujita *et al.* (2000) despite the differences in radioligand administration protocol. Therefore, no attempt was made to fit more than 3 compartments.

The bootstrap Monte Carlo estimate of the macroparameters, V_d, V_d', BP_1 and BP_2 and their SDs are tabulated in Tables 2 and 3. The correspondence between V_d and V_d' was very good ($V_d' = 0.98V_d - 0.01$; $r = 0.99$). A reduction in V_d and V_d' was observed in all regions during (-)-nicotine treatment ($\text{Evan}_{\text{nicotine}}$) as compared to the mean of the baseline studies ($\text{Evan}_{\text{baseline}}$, $\text{Evan}_{\text{post2}}$, $\text{Max}_{\text{baseline}}$, $\text{Max}_{\text{saline}}$, $\text{Max}_{\text{post1}}$): 31% in the cerebellum, 33% in the frontal cortex, and 57% in the thalamus for V_d. The variability of BP_1 was found to be as high as 46% and this was because of the low reliability in estimating k_2 to k_4 which are highly correlated. The reliability of BP_2 is generally

Table 2. Parameter estimates obtained from 2-compartment model fit for the treated baboon (Evan) and the control baboon (Max).

Study	2-compartment model†				
	K_1 (ml/ml/min)	k'_2 (1/min)	V'_d	AIC	SC
			Cerebellum		
$Evan_{baseline}$	0.176 ± 0.004	0.025 ± 0.001	7.14 ± 0.05	309.9	314.0 *
$Evan_{nicotine}$	0.197 ± 0.007	0.038 ± 0.001	5.26 ± 0.05	357.3	361.5 *
$Evan_{post1}$	0.193 ± 0.005	0.017 ± 0.001	11.65 ± 0.16	381.2	385.4 *
$Evan_{post2}$	0.188 ± 0.006	0.021 ± 0.001	8.80 ± 0.09	395.1	399.3 *
$Max_{baseline}$	0.203 ± 0.015	0.026 ± 0.002	7.70 ± 0.18	195.4	198.0 *
Max_{saline}	0.223 ± 0.012	0.031 ± 0.002	7.13 ± 0.11	379.8	384.0 *
Max_{post1}	0.303 ± 0.018	0.048 ± 0.003	6.37 ± 0.09	414.8	419.0
			Frontal Cortex		
$Evan_{baseline}$	0.179 ± 0.004	0.021 ± 0.001	8.67 ± 0.09	326.2	330.2 *
$Evan_{nicotine}$	0.188 ± 0.004	0.030 ± 0.001	6.32 ± 0.03	303.9	308.1 *
$Evan_{post1}$	0.188 ± 0.004	0.015 ± 0.001	12.98 ± 0.20	358.5	362.7 *
$Evan_{post2}$	0.187 ± 0.003	0.016 ± 0.000	11.49 ± 0.09	317.7	321.9 *
$Max_{baseline}$	0.253 ± 0.010	0.029 ± 0.001	8.72 ± 0.18	158.0	160.6 *
Max_{saline}	0.214 ± 0.005	0.023 ± 0.001	9.39 ± 0.13	376.1	380.3 *
Max_{post1}	0.257 ± 0.009	0.030 ± 0.001	8.55 ± 0.14	387.9	392.1 *
			Thalamus		
$Evan_{baseline}$	0.205 ± 0.004	0.010 ± 0.000	21.06 ± 0.37	333.6	337.7 *
$Evan_{nicotine}$	0.222 ± 0.005	0.024 ± 0.001	9.28 ± 0.11	381.8	386.0
$Evan_{post1}$	0.237 ± 0.003	0.007 ± 0.000	34.92 ± 0.72	314.9	319.1 *
$Evan_{post2}$	0.226 ± 0.004	0.009 ± 0.000	25.82 ± 0.45	337.9	342.1
$Max_{baseline}$	0.250 ± 0.020	0.012 ± 0.002	21.81 ± 1.28	168.8	171.4 *
Max_{saline}	0.221 ± 0.005	0.011 ± 0.000	21.14 ± 0.46	383.3	387.5 *
Max_{post1}	0.265 ± 0.009	0.017 ± 0.001	15.87 ± 0.41	411.5	415.7 *

Values are expressed as mean ± SD.
† Parameter value and SD are derived from bootstrap Monte Carlo technique.
* Nonparametric run test rejects the hypothesis of randomness ($P < 0.05$).

Table 3. Parameter estimates obtained from 3-compartment model fit for the treated baboon (Evan) and the control baboon (Max).

Study	3-compartment model†								
	K_1 (ml/ml/min)	k_2 (1/min)	k_3 (1/min)	k_4 (1/min)	V_d	BP_1	BP_2	AIC	SC
				Cerebellum					
$Evan_{baseline}$	0.222 ± 0.012	0.071 ± 0.020	0.068 ± 0.037	0.052 ± 0.008	7.23 ± 0.05	1.27 ± 0.55	3.87 ± 0.78	295.5	303.6
$Evan_{nicotine}$	0.217 ± 0.010	0.052 ± 0.008	0.014 ± 0.009	0.050 ± 0.006	5.31 ± 0.05	0.28 ± 0.13	1.13 ± 0.32	351.0	359.3
$Evan_{post1}$	0.246 ± 0.012	0.063 ± 0.015	0.083 ± 0.022	0.042 ± 0.005	11.91 ± 0.15	2.02 ± 0.57	7.85 ± 0.67	360.2	368.5
$Evan_{post2}$	0.235 ± 0.020	0.057 ± 0.012	0.051 ± 0.011	0.045 ± 0.011	8.99 ± 0.11	1.16 ± 0.31	4.75 ± 0.57	374.2	382.5
$Max_{baseline}$	0.273 ± 0.022	0.065 ± 0.005	0.034 ± 0.007	0.038 ± 0.005	7.94 ± 0.29	0.89 ± 0.15	3.72 ± 0.39	188.5	193.6 *
Max_{saline}	0.268 ± 0.022	0.059 ± 0.013	0.024 ± 0.012	0.040 ± 0.007	7.30 ± 0.12	0.60 ± 0.21	2.67 ± 0.49	354.4	362.8
Max_{post1}	0.350 ± 0.033	0.075 ± 0.016	0.020 ± 0.013	0.047 ± 0.028	6.59 ± 0.41	0.40 ± 0.17	1.83 ± 0.58	402.9	411.3
				Frontal Cortex					
$Evan_{baseline}$	0.228 ± 0.020	0.059 ± 0.011	0.051 ± 0.008	0.041 ± 0.008	8.91 ± 0.10	1.27 ± 0.27	4.94 ± 0.45	293.1	301.2
$Evan_{nicotine}$	0.238 ± 0.008	0.073 ± 0.010	0.054 ± 0.015	0.056 ± 0.005	6.39 ± 0.04	0.94 ± 0.20	3.06 ± 0.36	265.6	273.9
$Evan_{post1}$	0.228 ± 0.009	0.053 ± 0.005	0.093 ± 0.009	0.045 ± 0.005	13.23 ± 0.20	2.05 ± 0.21	8.88 ± 0.37	330.5	338.9
$Evan_{post2}$	0.239 ± 0.014	0.060 ± 0.013	0.078 ± 0.019	0.041 ± 0.007	11.77 ± 0.11	1.96 ± 0.51	7.67 ± 0.75	272.7	281.1
$Max_{baseline}$	0.299 ± 0.018	0.052 ± 0.004	0.024 ± 0.004	0.046 ± 0.006	8.88 ± 0.16	0.53 ± 0.09	3.06 ± 0.32	153.2	158.4 *
Max_{saline}	0.274 ± 0.022	0.062 ± 0.010	0.046 ± 0.005	0.040 ± 0.008	9.65 ± 0.13	1.17 ± 0.22	5.15 ± 0.55	359.5	367.9
Max_{post1}	0.309 ± 0.014	0.057 ± 0.004	0.024 ± 0.005	0.039 ± 0.005	8.77 ± 0.14	0.61 ± 0.09	3.30 ± 0.33	365.3	373.7 *
				Thalamus					
$Evan_{baseline}$	0.244 ± 0.007	0.056 ± 0.005	0.158 ± 0.019	0.041 ± 0.004	21.53 ± 0.34	3.89 ± 0.41	17.08 ± 0.66	313.1	321.2
$Evan_{nicotine}$	0.279 ± 0.015	0.069 ± 0.017	0.074 ± 0.030	0.056 ± 0.009	9.37 ± 0.13	1.30 ± 0.45	5.13 ± 0.84	373.4	381.8
$Evan_{post1}$	0.270 ± 0.004	0.052 ± 0.003	0.251 ± 0.013	0.043 ± 0.003	34.43 ± 0.72	5.86 ± 0.44	30.25 ± 0.84	307.0	315.4
$Evan_{post2}$	0.263 ± 0.006	0.052 ± 0.005	0.186 ± 0.015	0.044 ± 0.004	26.27 ± 0.45	4.22 ± 0.45	21.20 ± 0.73	328.3	336.7
$Max_{baseline}$	0.281 ± 0.017	0.051 ± 0.004	0.134 ± 0.023	0.042 ± 0.004	23.03 ± 0.84	3.20 ± 0.43	17.50 ± 1.11	164.9	170.1 *
Max_{saline}	0.261 ± 0.008	0.053 ± 0.004	0.146 ± 0.010	0.044 ± 0.004	21.58 ± 0.43	3.34 ± 0.30	16.59 ± 0.58	374.0	382.4
Max_{post1}	0.329 ± 0.020	0.056 ± 0.008	0.075 ± 0.012	0.043 ± 0.008	16.30 ± 0.47	1.79 ± 0.35	10.37 ± 0.95	402.5	410.8

Values are expressed as mean ± SD.
† Parameter value and SD are derived from bootstrap Monte Carlo technique.
* Nonparametric run test rejects the hypothesis of randomness ($P < 0.05$).

better than that of BP_1, with CV <20% except for the cerebellum curves of $Evan_{nicotine}$ and Max_{post1}.

The randomness of the data point distribution above the fitted curve was tested by the nonparametric run test. With the exception of the thalamus curves during nicotine treatment ($Evan_{nicotine}$) and post-(-)-nicotine treatment ($Evan_{post2}$), and the cerebellum curve of Max_{post1}, the hypothesis of randomness was rejected for all other 2-compartment model fits. As for 3-compartment model fitting, the hypothesis was rejected in Max at baseline level ($Max_{baseline}$) and the frontal cortex curve of Max_{post1}. Figure 3 shows the fitted curves obtained for the frontal cortex of $Max_{baseline}$, where the hypothesis of randomness was rejected for 3-compartment model fit. Inspection of the plot showed that the results were not caused by the inadequacy of the 3-compartment model but the problem with the data. There were technical problems during the synthesis of the radioligand for the study of post saline treatment in Max (Max_{post1}), as the administered activity was only about half that of the other studies (Table 1), which may possibly account for the atypical results seen with the frontal cortex

curve, although it is not clear whether these technical difficulties could have affected the tracer kinetics and the observed differences. To test the hypothesis of 3-compartment model fit provides a significantly better fit to the data over 2-compartment model fit, the F-statistic was applied and it suggested that the hypothesis could not be rejected in all cases. This finding was also supported by the AIC and SC, as presented in Tables 2 and 3.

4. CONCLUSIONS

Our results demonstrate that, with the modelling strategies used, reliable fits could be obtained with a 3-compartment model which provided a significantly improved fitting as compared to the 2-compartment model, despite poor identifiability in some parameters. Adequate reliability for the K_1 and macroparameter V_d was obtained with the 3-compartment model. The 2-compartment model failed to fit the data completely and hence introduced biases, in particular, the K_1 estimate compared to the 3-compartment model. The higher reliability of the 2-compartment model may have advantage for the generation of parametric images.

5. REFERENCES

Akaike, H. (1974). A new look at the statistical model identification. *IEEE Trans. Automatic Control* **AC-19**, 716–723.

Chefer, S. I., A. G. Horti, K. S. Lee, A. O. Koren, D. W. Jones, J. G. Gorey, J. M. Links, A. G. Mukhin, D. R. Weinberger and E. D. London (1998). *In vivo* imaging of brain nicotinic acetylcholine receptors with 5-[^{123}I]iodo-A-85380 using single photon emission computed tomography. *Life Sci.* **63**, PL355–PL360.

Corrigall, W. A., K. B. J. Franklin, K. M. Coen and P. B. S. Clarke (1992). The mesolimbic dopaminergic system is implicated in the reinforcing properties of nicotine. *Psychopharmacology* **107**, 285–289.

Eberl, S., I. Kanno, R. R. Fulton, A. Ryan, B. F. Hutton and M. J. Fulham (1996). Automated interstudy image registration technique for SPECT and PET. *J. Nucl. Med.* **37**, 137–145.

Fujita, M., G. Tamagnan, S. S. Zoghbi, M. S. Al-Tikriti, R. M. Baldwin, J. P. Seibyl and R. B. Innis (2000). Measurement of $\alpha_4\beta_2$ nicotinic acetylcholine receptors with [^{123}I]5-I-A-85380 SPECT. *J. Nucl. Med.* **41**, 1552–1560.

Hudson, H. M. and R. S. Larkin (1994). Accelerated image reconstruction using ordered subsets of projection data. *IEEE Trans. Med. Imag.* **13**, 601–609.

Kassiou, M., S. Eberl, S. R. Meikle, A. Birrell, C. Constable, M. J. Fulham, D. F. Wong and J. L. Musachio (2001). In vivo imaging of nicotinic receptor upregulation following chronic (-)-nicotine treatment in baboon using SPECT. *Nucl. Med. Biol.* **28**, 165–175.

Landaw, E. M. and J. J. DiStefano, III (1984). Multiexponential, multicompartmental, and noncompartmental modeling. II: Data analysis and statistical considerations. *Am. J. Physiol.* **246**, R665–R677.

Laruelle, M., E. Wallace, J. P. Seibyl, R. M. Baldwin, Y. Zea-Ponce, S. S. Zoghbi, J. L. Neumeyer, D. S. Charney, P. B. Hoffer and R. B. Innis (1994). Graphical, kinetic, and equilibrium analyses of in vivo [^{123}I]β-CIT binding to dopamine transporters in healthy human subjects. *J. Cereb. Blood Flow Metab.* **14**, 982–994.

Levin, E. D. and J. E. Rose (1995). Acute and chronic nicotinic interactions with dopamine systems and working memory performance. *Ann. N.Y. Acad. Sci.* **757**, 245–252.

Mintun, M. A., M. E. Raichle, M. R. Kilbourn, G. F. Wooten and M. J. Welch (1984). A quantitative model for the in vivo assessment of drug binding sites with PET. *Ann. Neurol.* **15**, 217–227.

Molina, P. E., Y. S. Ding, F. I. Caroll, F. Liang, N. D. Volkow, N. Pappas, M. Kuhar, N. Abumrad, S. J. Gatley and J. S. Fowler (1997). Fluoronorchloroepibatidine: preclinical assessment of acute toxicity. *Nucl. Med. Biol.* **24**, 743–747.

Musachio, J. L., U. Scheffel, P. A. Finley, Y. Zhan, T. Mochizuki, H. N. Wagner, Jr. and R. F. Dannals (1998). 5-[I-125/123]iodo-3(2(S)-azetidinylmethoxy)pyridine, a radioiodinated analog of A-85380 for *in vivo* studies of central nicotinic acetylcholine receptors. *Life Sci.* **62**, PL351–PL357.

Musachio, J. L., V. L. Villemagne, U. A. Scheffel, R. F. Dannals, A. S. Dogan, F. Yokoi and D. F. Wong (1999). Synthesis of an I-123 analog of A-85380 and preliminary SPECT imaging of nicotinic receptors in baboon. *Nucl. Med. Biol.* **26**, 201–207.

Narita, Y., H. Iida, S. Eberl and T. Nakamura (1997). Monte Carlo evaluation of accuracy and noise properties of two scatter correction methods for ^{201}Tl cardiac SPECT. *IEEE Trans. Nucl. Sci.* **44**, 2465–2472.

Nybäck, H., C. Hallidin, A. Åhlin, M. Curvall and L. Eriksson (1994). PET studies of the uptake of (S)- and (R)-[^{11}C]nicotine in the human brain: Difficulties in visualizing specific receptor binding *in vivo*. *Psychopharmacology* **115**, 31–36.

Perry, E. K., C. M. Morris, J. A. Court, A. Cheng, A. F. Fairbairn, I. G . Mckeith, D. Irving, A. Brown and R. H. Perry (1995). Alteration in nicotine binding sites in Parkinson's disease, Lewy body dementia and Alzheimer's disease: possible index of early neuropathology. *Neuroscience* **64**, 385–395.

Press, W. H., S. A. Teukolsky, W. T. Vetterling and B. P. Flannery (1992). *Numerical Recipes in C. The Art of Scientific Computing*. Cambridge University Press. New York.

Schwarz, G. (1978). Estimating the dimension of a model. *Ann. Stat.* **6**, 461–464.